Laser Surface Hardening of Austenitic Stainless Steel

S.M. Levcovici, D.T. Levcovici, V. Munteanu, M.M. Paraschiv, and A. Preda

(Submitted 22 March 2000)

For the purpose of studying the possibilities of increasing the wear resistance, keeping a high level of corrosion strength, austenitic stainless steel specimens mainly containing 19.2%Cr and 9.4%Ni were two-step surface alloyed using added materials (AMs) with hard particles of carbides (WC), nitrides (TiN), and borides (TiB_2). The simultaneous melting of AM and surface layer was performed by a CO_2 continuous wave laser on a numerically controlled X-Y table. On these specimens, the microstructural characteristics, microhardness, and depth of the molten zone were determined, which allowed definition of the AM with the best hardening effect. The research continued by two-step laser surface alloying of the same base material with different effective AM quantities. The specimens were processed by continuous wave laser radiation, by multiple-pass with 35% overlap. The alloyed layers were described by light optical microscopy, x-ray diffractometry, flash spectrometry, and hardness measurement. The conditions to obtain compact surface layers with 2.5 to 3 times higher hardness than the base material were determined.

Keywords austenite stainless steel, borides, carbides, laser hardening, nitrides, surface modification

1. Introduction

In many industrial plants, for the processing and storing of the fluid materials, the hydrodynamic transport processes were increased for economical reasons. The question that arises is should the parts made of austenitic stainless steel present not only suitable corrosion strength, but also a higher strength to the abrasive action of the complex environment where they operate? It is known that solid-state heat-treatment processes cannot harden the austenitic stainless steel. Therefore, research works were conducted to determine the most effective methods of surface hardening by local melting.[1,7] In this report, the results of the research works performed for the surface hardening of the austenitic stainless steel by simultaneous melting of the surface layer and several AMs with hard particles of carbides (WC), nitrides (TiN), and borides (TiB_2) are shown. The local melting was performed using a CO_2 continuous wave laser provided with a numerically controlled X-Y table. For the laboratory experiments, the light optical microscope with automatic image analysis, flash spectrometer, x-ray diffractometer, microhardness meter, *etc.* was used.

2. Methods

The experiments for the determination of the hardening conditions of austenitic stainless steel with 0.09% C, 1.7% Mn, 0.7% Si, 19.2% Cr, 9.4% Ni, and 0.4% Ti were made on plates of $50 \times 40 \times 20$ mm^3. The AM was made as paste by mixing a part of hydroxiethyl cellulose with three parts of powder with the composition shown in Table 1.

After paste covering and drying, the specimens were mounted on a numerically controlled X-Y table and irradiated by CO_2 continuous wave laser, under argon protection. The radiation power $P = 820$ W, the laser beam diameter on the specimen surface $d_s = 1.2$ mm (by a lens of 127 mm focal distance), and the scanning rate $v = 1$, 3, and 5.5 mm/s were used. The microstructural characteristics, depth, and microhardness of the alloyed zone were determined on the specimen cross section metallographically prepared by optical microscopy. Different quantities were predeposited on the same base material using the **A**. The specimens were mounted on the numerically controlled X-Y table and multiple-pass scanned with the rate $v = 10$ mm/s and the overlapping degree $s = 35\%$. The continuous wave radiation was used with the power $P = 1300$ W, the beam diameter $d_s = 1.2$ mm, and argon protection. The surface layers thus obtained were described by spectral analysis, x-ray diffractometry, and hardness measurements (HV_{98}). The metallographic analysis by light optical microscopy was performed in the layer's cross section.

3. Results and Discussions

The results of the metallographic analysis and the hardness measurements made on single bands processed with different scanning rates ($P = 820$ W, and $d_s = 1.2$ mm) are shown in Table 2, (A: austenite; E: interdendritic eutectic; P: pores; and C: cracks). The analysis on the light optical microscope showed

Table 1 AM composition

	Composition in wt. %				
AM code	**WC**	**TiN**	**TiB_2**	**Co**	**Si**
A	73	. . .	. . .	12	15
B	65	25	. . .	10	. . .
C	65	. . .	25	10	. . .

S.M. Levcovici, "Dunărea de Jos" University, 6200 Galatzi, Romania; and **D.T. Levcovici, V. Munteanu, M.M. Paraschiv**, and **A. Preda**, The Research and Design Institute, "Uzinsider Engineering" S.A., 6200 Galatzi, Romania.

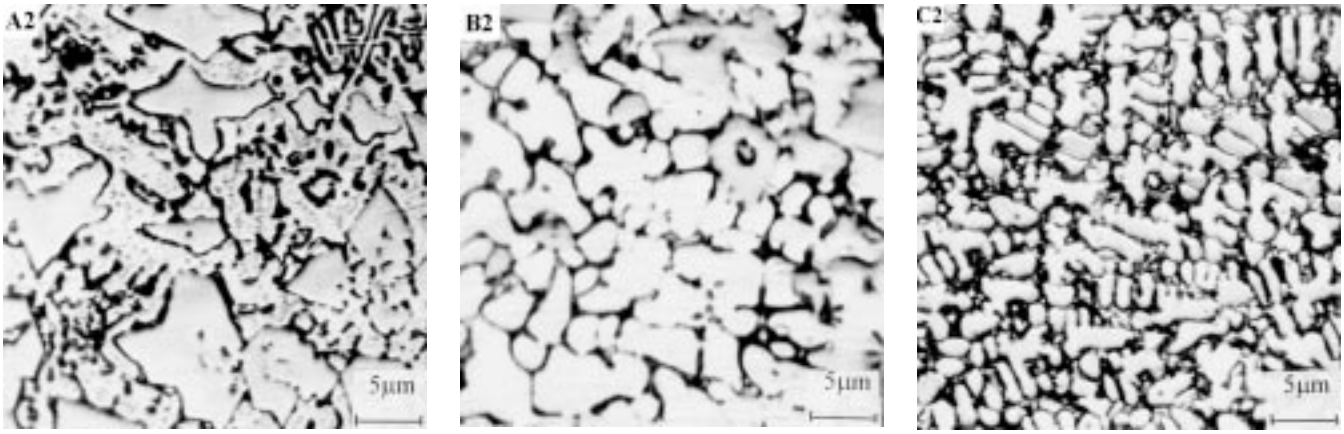

Fig. 1 The microstructure of the **A2**, **B2**, and **C2** alloyed layers. 2% nital attack

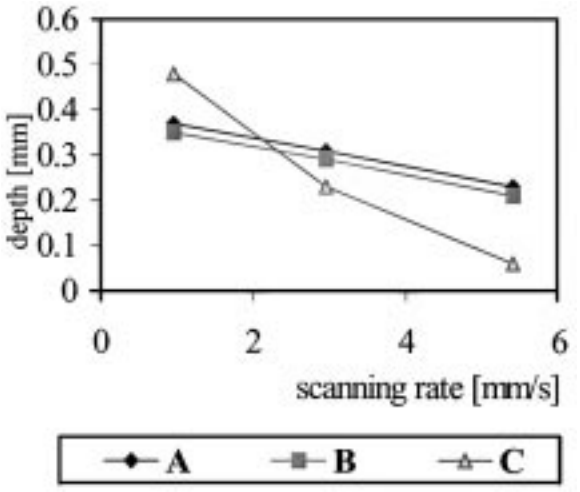

Fig. 2 The variation of depth of the alloyed zone with the scanning rate

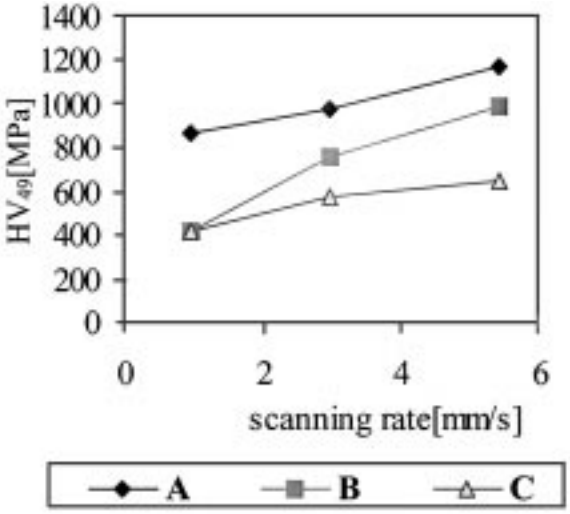

Fig. 3 The variation of hardness with the scanning rate

Table 2 The metallographic analysis and the hardness measurements

AM	Regime code	ν (mm/s)	Alloyed zone depth (mm)	HV_{49} (MPa)	Microstructural characteristics
	A1	1	0.37	8640	A + E
A	A2	3	0.32	9680	A + E + WC
	A3	5.5	0.23	11,640	A + E + WC
	B1	1	0.35	4200	A + E + TiN
B	B2	3	0.26	7530	A + E + TiN, P, C
	B3	5.5	0.18	9870	A + E + TiN, P, C
	C1	1	0.45	4110	A + E + TiB_2, P, C
C	C2	3	0.23	5740	A + E + TiB_2, P, C
	C3	5.5	0.15	6500	A + E + TiB_2, P, C

that the **A** AM led to compact layers, with complete dissolution of WC particles at the **A1** regime, and WC recrystallized particles at **A2** and **A3** regimes, TiN and TiB_2, proved a high stability in all the experimented regimes, the presence of nondissolved particles being noticed (Fig. 1). At high scanning rates, the layers alloyed with the **B** AM showed pores and cracks. Such defects were present in all the layers alloyed with the **C** AM.

In Fig. 2 and 3, the variations of depth of the alloyed zone as well as its average hardness with a scanning rate are shown, and in Fig. 4 to 6, the microhardness variations with the alloyed zone depth for each AM and scanning rate are shown.

The **A** AM provides the maximum alloying depth. Both WC and Co reduce significantly the specific heat of the stainless steel and provide the highest surface temperatures, promoting WC particle dissolution, and W, Co, and Si increase the thermal conductivity of the melt. Formulas **B** and **C** especially result in lower alloying depths. TiN and TiB_2, particularly, increase the specific heat of the melt and reduce the surface temperature and, as a result, the dissolution degree of these particles. The HV_{49} hardness on the alloyed surface (Fig. 3) is maximum for the formula **A** and minimum for the formula **C**.

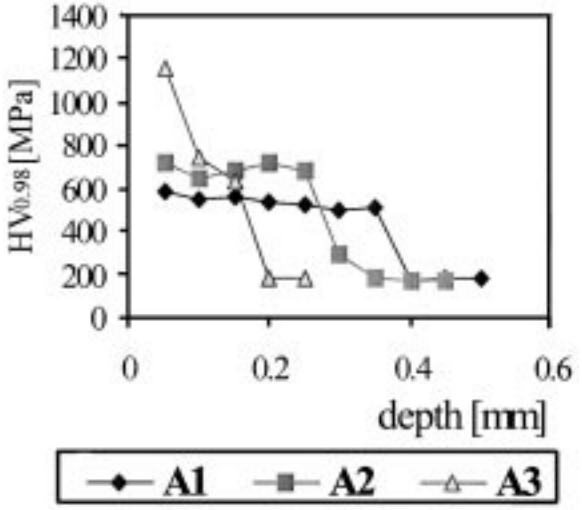

Fig. 4 The variation of microhardness in the depth of the alloyed layer for **A** added material

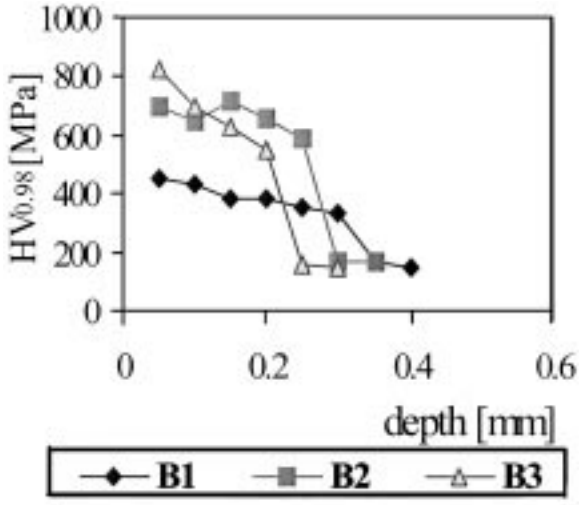

Fig. 5 The variation of microhardness in the depth of the alloyed ayer for **B** added material

As a result, the experiments of hardening the austenitic stainless steel in the surface layer were developed with the **A** AM.

In Table 3, the quantity of predeposited AM, the average chemical composition, and hardness obtained on the surface of the multiple-pass melting layer are presented. Compared to the hardness measured in the alloyed layer resulting from single scanning, lower values determined by the self-tempering phenomena, corresponding to the 35% overlapping degree, were obtained in the multiple-pass scanning alloyed layers.

The phase qualitative analysis by x-ray diffraction in CuK_α, U = 25 A; I = 15 mA, with the variation of diffraction angle 2θ in the range 15- to 120° and rotation speed of the goniometer

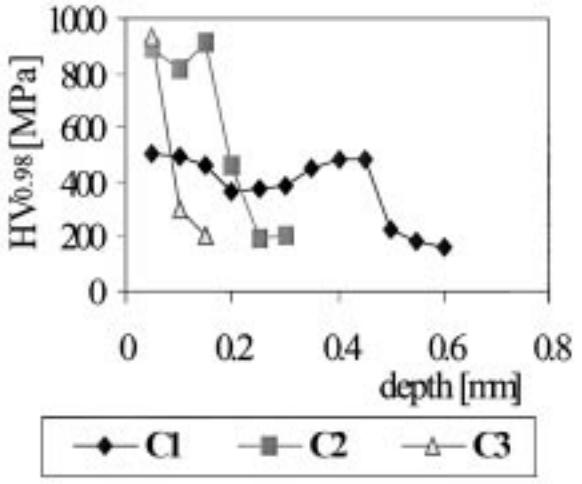

Fig. 6 The variation of microhardness in the depth of the alloyed layer for **C** added material

Table 3 The variation of the average chemical composition and hardness with the quantity of predeposited A AM

AM quantity × 10^{-3} g/cm^2	Chemical composition, %							HV_{98} (MPa)
	C	Si	Cr	Ni	W	Co	Ti	
. . .	0.09	0.7	19.2	9.4	. . .	. . .	0.40	1920
35	0.97	1.4	16.3	8.3	16.5	0.9	0.14	5000
56	1.39	3.2	15.9	8.2	21.5	1.2	0.10	6340
71	1.43	3.5	15.9	8.2	21.8	1.3	0.04	6550

ω = 2° min^{-1}; 1; 1; and 0.5—pointed out the presence of the following phases: $Cr_{23}C_6$, Cr_7C_3, Fe_3C, Fe_3W_3C, Fe_2W, Feα, Feγ, W_2C-β, WC, and Co_2C in each layer.

For AM = 35 × 10^{-3} g/cm^2, the chemical homogenization of the melt favors the occurrence of Cr_7C_3 and $Cr_{23}C_6$ carbides, while for AM = 56 × 10^{-3} g/cm^2, only $Cr_{23}C_6$ forms. The increase of the AM quantity is followed by the increase of the martensite quantity, WC, W_2C, Fe_3W_3C, and $Cr_{23}C_6$ with a hardening effect. The variation of the maximum value of the relative intensity with the diffraction angle for AM = 56 × 10^{-3} g/cm^2 is shown in Fig. 7.

General views of the microstructure in the cross section of the laser-alloyed layers are shown in Fig. 8 for AM = 35 × 10^{-3} g/cm^2, AM = 56 × 10^{-3} g/cm^2, and AM = 71 × 10^{-3} g/cm^2, respectively. An increase of the melting depth instability with the increase of the predeposited quantity is found. Also, the increase of the AM predeposited quantity caused the emphasis of the microstructure finishing degree both in the center and at the base of the cross section of the alloyed zone (Fig. 9 and 10).

With the increase of the hard phase content of carbide- and intermetallic compound type, the hardness of the alloyed layer increased 2.5 to 3 times compared with the base material.

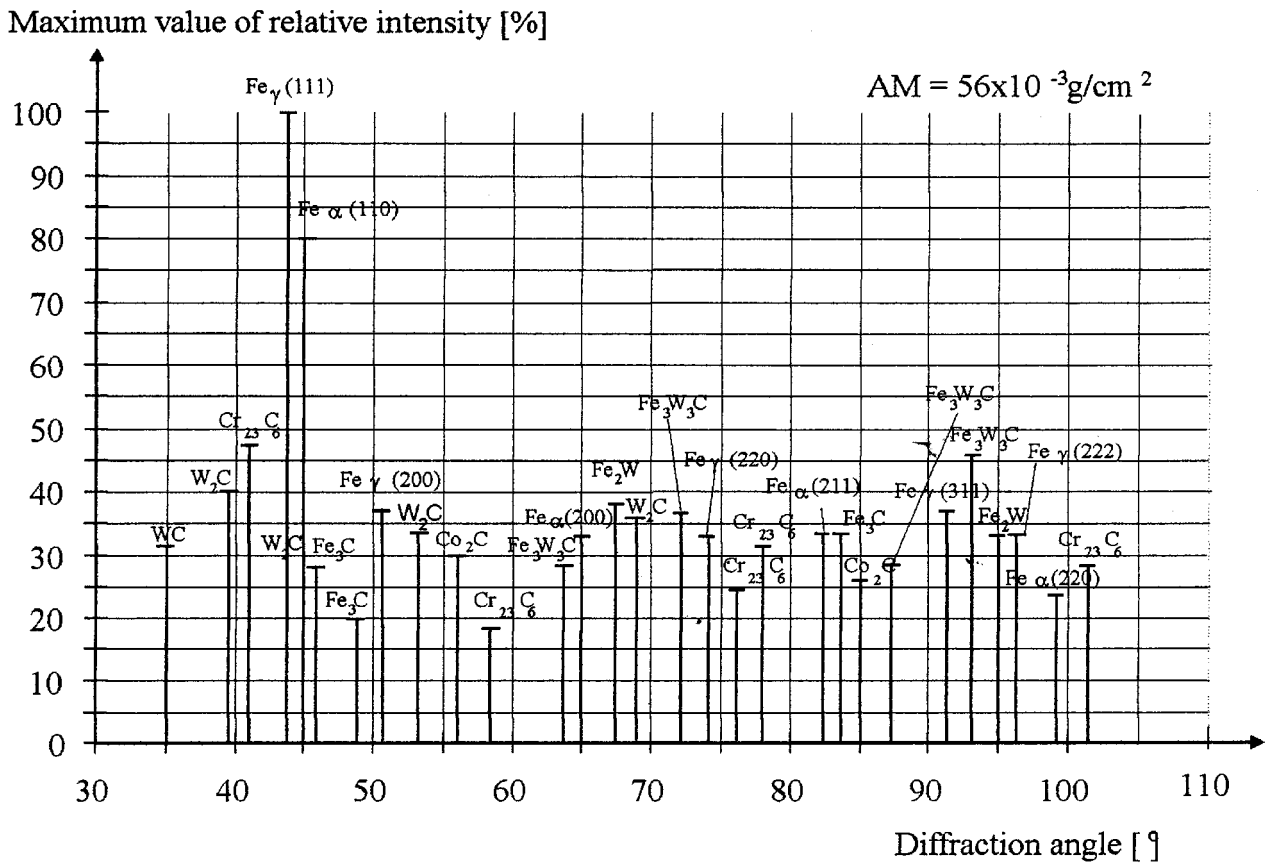

Fig. 7 The variation of maximum value of the relative intensity with the diffraction angle

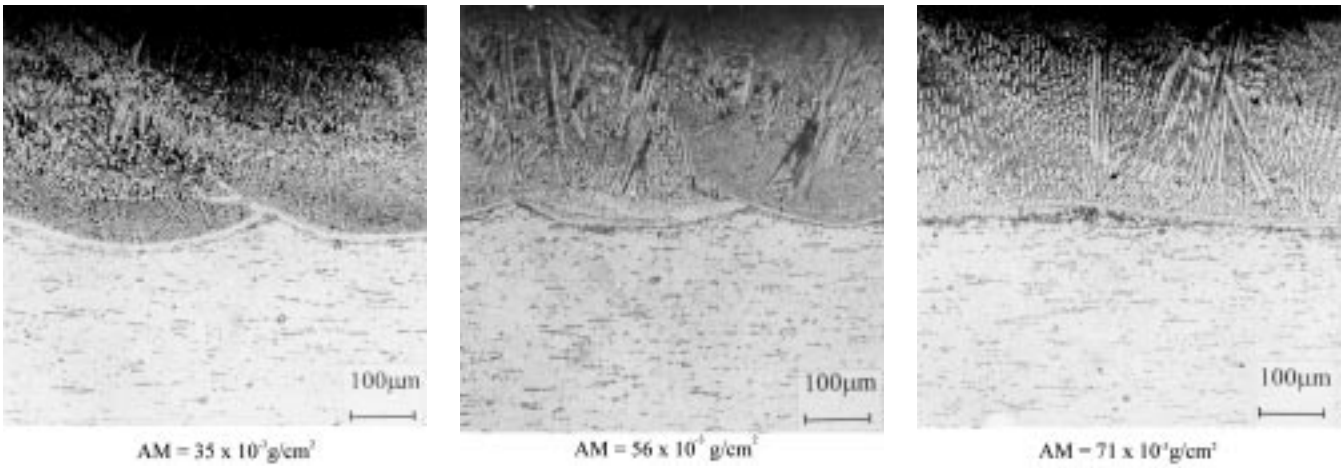

Fig. 8 The microstructure in the cross section. 2% nital attack

4. Conclusions

By laser surface alloying using the two-step procedure with the AM consisting of one part hydroxiethyl cellulose and three parts powder with 73% WC + 12% Co + 15% Si, continuous and smooth alloyed layers can be obtained, showing average hardnesses up to 5 times higher than the base material.

Due to the self-tempering effects determined by the multiple-pass scanning with 35% overlapping, layers alloyed with the same AM have average hardnesses of 2.5 to 3 times higher than the base material. With the increase of the predeposited AM

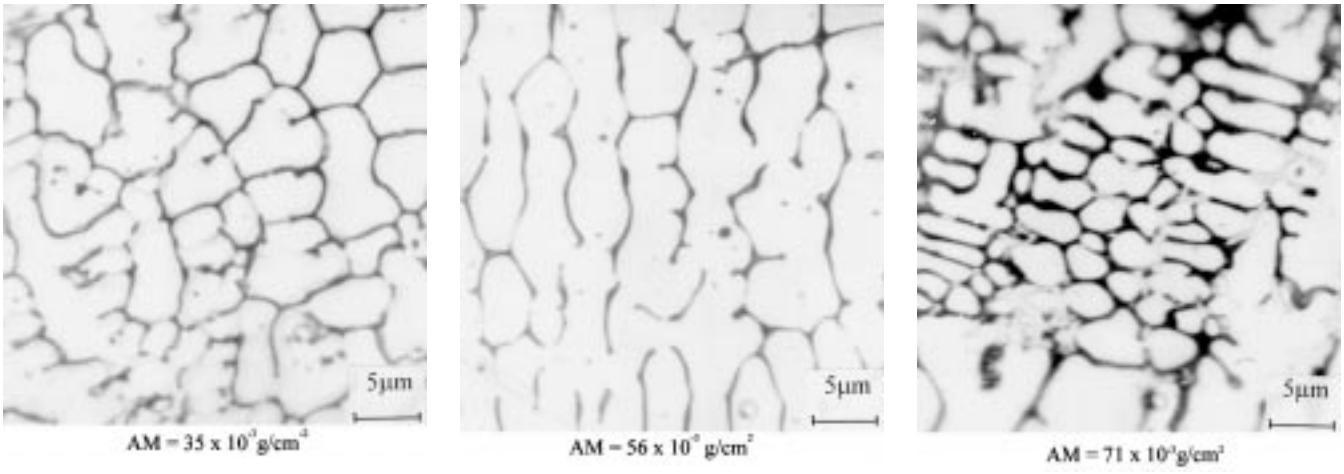

Fig. 9 The microstructure in the center of the cross section. 2% nital attack

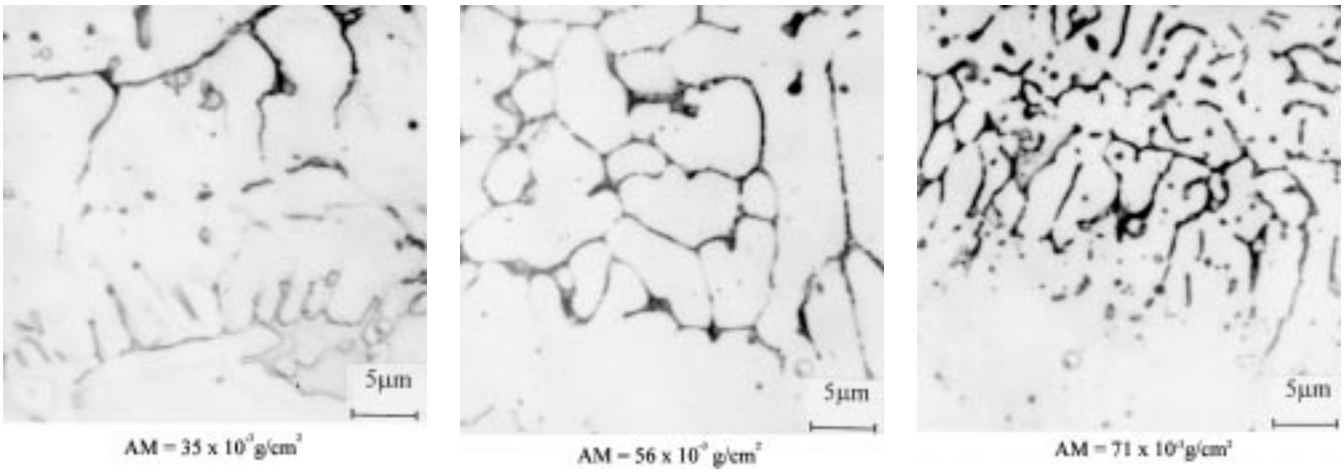

Fig. 10 The microstructure at the base of the cross section. 2% nital attack

quantity, a restriction of the new alloying element assimilation degree, and hence an efficiency limit of the experimental hardening procedure, was found.

References

1. G. Barton, H.W. Bergmann, B.L. Mordike, and N. Gros: *Laser Materials Processing II, SPIE*, 1988, vol. 455, p. 113.
2. P.E. Denney: *Proc. Eur. Conf. Laser Treatment of Materials, ECLAT '92*, edited by B.L. Mordike, Götingen, 1992, p. 71.
3. B. Grünenwald, J. Schen, F. Dausinger, and S. Novotny: *Proc. Conf. Laser Treatment of Materials, ECLAT '92*, edited by B.L. Mordike, Götingen, 1992, p. 411.
4. S.M. Levcovici, D.T. Levcovici, V. Gologan, and L. Farkas: *Proc. Conf. on Advanced Materials and Processes and Applications, EUROMAT '97*, edited by L.A.J.L. Sarton and H.B. Zeedijk, Zwijndrecht, p. 131.
5. D.T. Levcovici, V. Munteanu, S.M. Levcovici, O. Mitoseriu, L. Benea, and M.M. Paraschiv: *Materials and Manufacturing Processes*, vol. 14, No. 4, edited by T.S. Sudarshan and T.S. Srivatsan, New York, 1999, p. 475.
6. E. Lugscheider, H. Bolender, and H. Krappitz: *Proc. Eur. Conf. on Laser Treatment of Materials, ECLAT '92*, edited by B.L. Mordike, Götingen, 1992, p. 369.
7. K. Masaski and M. Hiderki: *Material Processing—The Sumitomo Search No. 41*, 1990, p. 39.